

Whole-Mars Decompression Dynamics

J. Marvin Herndon, Ph.D.

Transdyne Corporation, San Diego, CA 92131 USA

ABSTRACT

Whole-Mars Decompression Dynamics is a new planetary science paradigm that follows from observations that Mars, like Earth, primarily formed by condensing and raining out from within a giant gaseous protoplanet, whose massive shell of gases and ices compressed the rocky planet, but was subsequently stripped away by the super-intense T-Tauri phase solar winds associated with thermonuclear ignition of the sun. For a brief period, perhaps one billion years, Mars' nuclear fission planetocentric reactor produced the planet's magnetic field and supplied the lost heat of protoplanetary compression which enabled whole-Mars decompression to proceed. Through the process of mantle decompression thermal tsunami, the stored energy of protoplanetary compression also heated the crust and provided a thermal barrier to the downward percolation of water. Presumably contemporaneous with demise of the magnetic field, the whole-Mars decompression process subsided, concomitantly transforming Mars from warm and wet to cold and dry. Whole-Mars Decompression Dynamics provides different possible interpretations of Martian features and events, including the perimeter-features of Valles Marineris being circum-perimeter tears like Norwegian fjords, surface pits being the consequence of hydrogen geysers like on Mercury, and implications where one might hope to find Martian hydrocarbon deposits.

Keywords: Protoplanetary, Whole-Earth Decompression Dynamics, Martian life, georeactor, Valles Marineris, Fjords.

INTRODUCTION

The prime impetus of scientific investigations of Mars is the search for water, as a potential harbinger of life and as a resource for human exploration.

Presently, only traces of water are present on Mars' surface, although observational evidence suggests the presence of copious amounts of surface water on Mars during its early history. What circumstances allowed its presence and subsequently caused its near-absence? These are the questions I address here, however, not by considering Mars as an entity unto itself, but in light of evidence related to the formation of the terrestrial planets generally, and Earth particularly, as set forth in my new indivisible solar system paradigm [1]. That indivisible paradigm accounts for the differences observed among the terrestrial planets and accounts for the asteroid belt as well.

In 1944, Eucken [2] employed thermodynamic considerations to investigate Earth's formation from within a giant gaseous protoplanet. Notably, he discovered that at high pressures Earth's core of molten iron would condense before mantle silicates from an atmosphere of solar composition. Complete condensation would yield a Jupiter-like layer of gases and ices.

In 1976, Suess and I [3] confirmed Eucken's calculations and demonstrated that primordial condensation at high pressures and high temperatures would yield a condensate with a state of oxidation similar to primitive enstatite chondrites, provided the condensate was separated and prevented from further reaction with primordial gases at lower temperatures. Subsequently, I connected Earth's condensation to the circumstances described by Eucken [2] and Suess and I [3] by relating ratios of mass of mineralogically determined parts of a primitive enstatite chondrite to geophysically determined parts of the Earth [4-7], as shown in Table 1 from [7] and illustrated schematically in Figure 1.

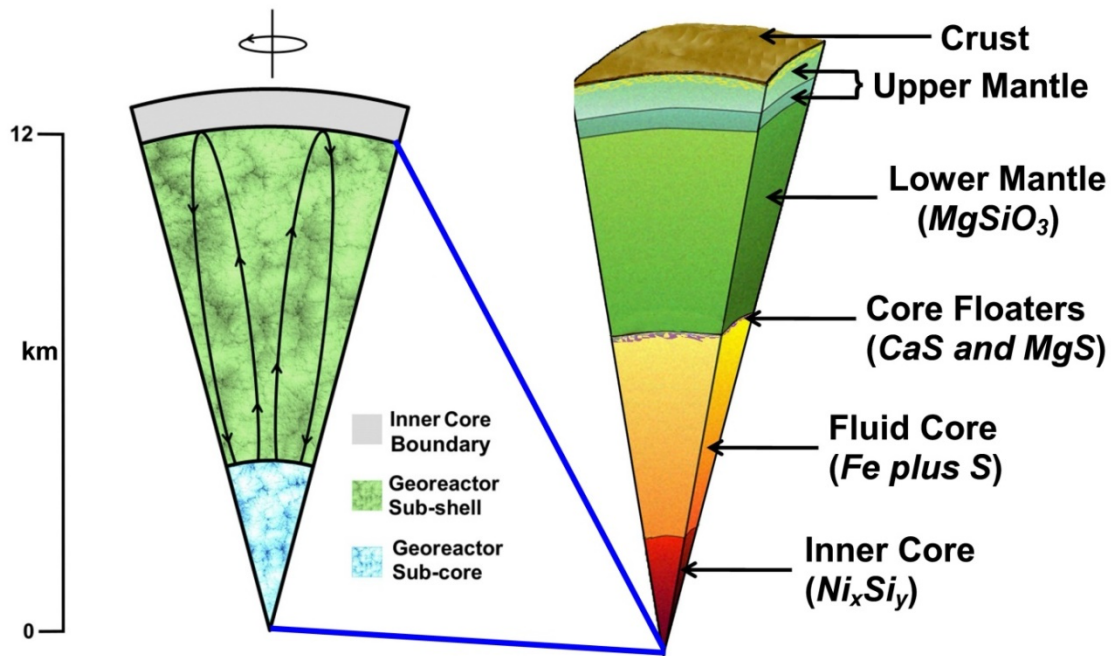


Figure 1. Major portions of the Earth's interior from [8] based on [9-17] and the relationships shown in Table 1. Also, schematic representation of Earth's nuclear fission georeactor with planetary rotation and fluid motions are indicated separately; their resultant motion is not shown

Table 1. Fundamental mass ratio comparison between the endo-Earth (lower mantle plus core) and the Abee enstatite chondrite. Above a depth of 600 km seismic data [18] indicate data layers suggestive of veneer, possibly formed by the late addition of more oxidized chondritic and cometary matter, whose compositions cannot be specified at this time.

Fundamental Earth Ratio	Earth Ratio Value	Abee Ratio Value
lower mantle mass to total core mass	1.49	1.43
inner core mass to total core mass	0.052	theoretical 0.052 if Ni ₃ Si 0.057 if Ni ₂ Si
inner core mass to lower mantle + total core mass	0.021	0.021
D'' mass to total core mass	0.09*	0.11**
ULVZ† of D'' CaS mass to total core mass	0.012****	0.012**

Calculated assuming average thickness of 200 km. ** = avg. of Abee, Indarch, and Adhi-Kot enstatite chondrites. D'' is the "seismically rough" region between the fluid core and lower mantle. ULVZ *** is the "Ultra Low Velocity Zone" of D''. *Calculated assuming average thickness of 28 km. Data from references [19-21]**

In 1952, Birch [22] discussed at length the importance of chondrite meteorites for understanding Earth's internal composition, but lamented on the difficulty of ascertaining which of the many different meteorites resembles Earth. I obviated that difficulty by relating parts of meteorites to parts of the Earth by mass ratios [4-7] and discovered that the inner 82% of Earth resembles the Abee enstatite chondrite. Previously, for decades scientists had assumed Earth resembles an ordinary chondrite, one of the most abundant meteorites that have fallen to Earth.

As previously noted [23], the abundances of major elements in chondrites have been expressed in the literature as ratios, usually relative to silicon (E_i/Si) and occasionally relative to magnesium (E_i/Mg). By expressing Fe-Mg-Si elemental abundances as atom (molar) ratios relative to iron (E_i/Fe), as shown for comparison in Figure 2, I discovered a fundamental relationship bearing on the origin of ordinary chondrite matter [24].

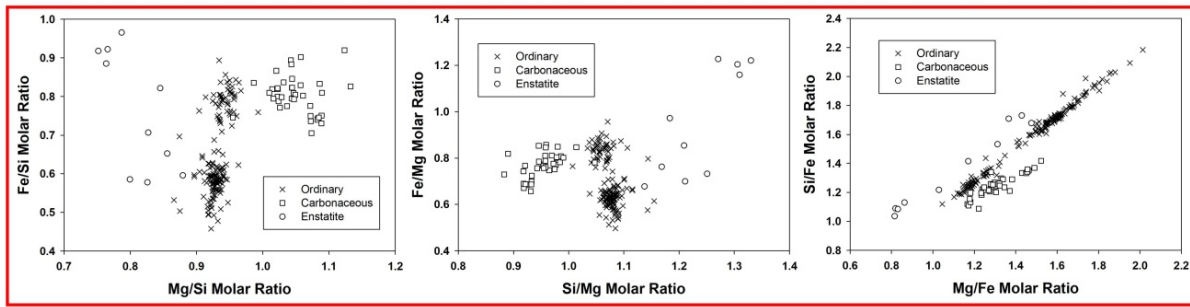


Figure 2. The same major element chondrite data plotted three different ways. The plot on the right, originated by me, shows a relationship that is not evident in the other plots

The rightmost plot of Figure 2 is presented in greater detail in Figure 3 which shows atom (molar) ratios of Mg/Fe vs. Si/Fe from analytical data on 10 enstatite chondrites, 39 carbonaceous chondrites, and 157 ordinary chondrites. The well-defined, linear regression lines are evident only when normalized to Fe, not to Si or Mg. The ordinary chondrite points scatter about a line that intersects the other two lines. Points on the ordinary chondrite line can be represented by mixtures of the two intersecting compositions, point A: *primitive*, and point B: *planetary*. For more detail, see [24]. Near points of intersection, 95% confidence intervals are shown.

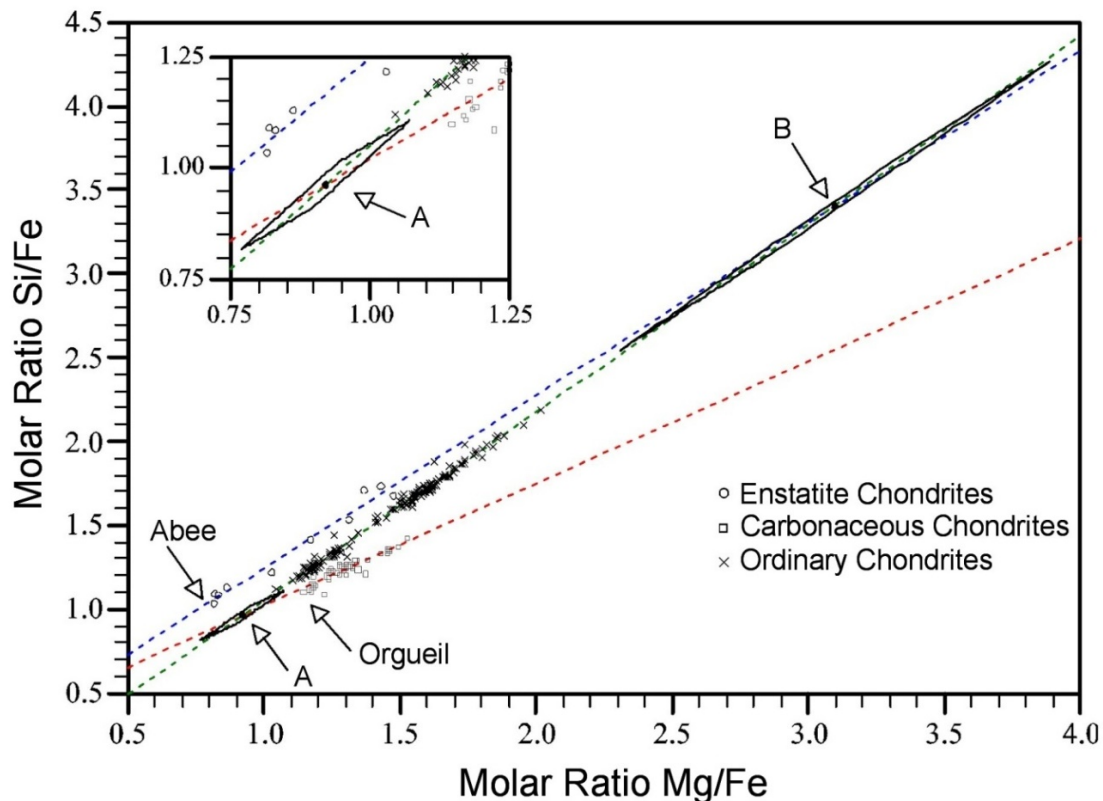


Figure 3. Atom (molar) ratios of Mg/Fe vs. Si/Fe from analytical data on 10 enstatite chondrites, 39 carbonaceous chondrites, and 157 ordinary chondrites. Least squares linear regression lines are shown. Near points of intersection, 95% confidence intervals are shown. For references and more detail, see [23]

The relationship I discovered, shown in Figure 3, implies that ordinary chondrites were derived from mixtures of two components, representative of two other types of matter, designated *primitive* and *planetary* and defined by the intersecting points along the ordinary chondrite line. The ordinary chondrites consist of mixtures of a relatively undifferentiated carbonaceous-chondrite-like *primitive* component and a partially differentiated enstatite-chondrite-like *planetary* component where its molar (atom) iron content is only one third that of its magnesium and its silicon content.

The *planetary* component, I posited, was the partially differentiated matter stripped from Mercury's protoplanet by the sun's thermonuclear-ignition T-Tauri super-intense solar winds where, in the region between Mars and Jupiter, it fused with in-falling primitive matter [23]. The ordinary-chondrite parent matter thus formed populated the asteroid belt (Figure 4) and added a veneer that fell onto the outer portion of Earth, and to a greater relative degree, onto Mars.

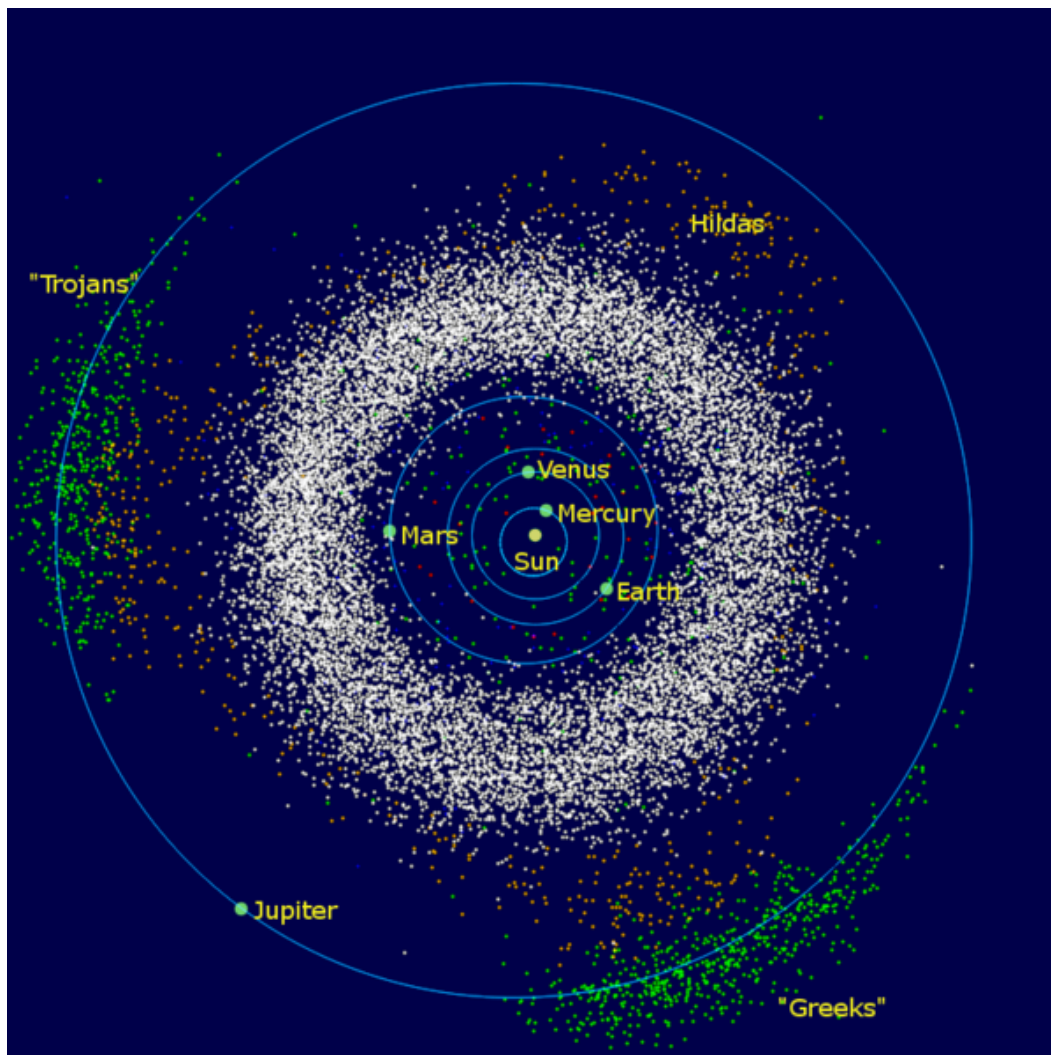


Figure 4. The inner solar system showing the plethora of asteroids. From [24].

Several lines of evidence validate the protoplanetary theory of solar system formation [25]. Although the popular planetesimal theory does not account for solar system formation, some of its elements added a veneer of oxidized material to the outer portions of Earth, especially oxidized iron which is critical for the development of life. The high oxidized iron content of the Martian regolith, giving Mars its red color (Figure 5), suggests considerably greater “veneer” additions due to Mars’ relatively closer proximity to the asteroid belt.

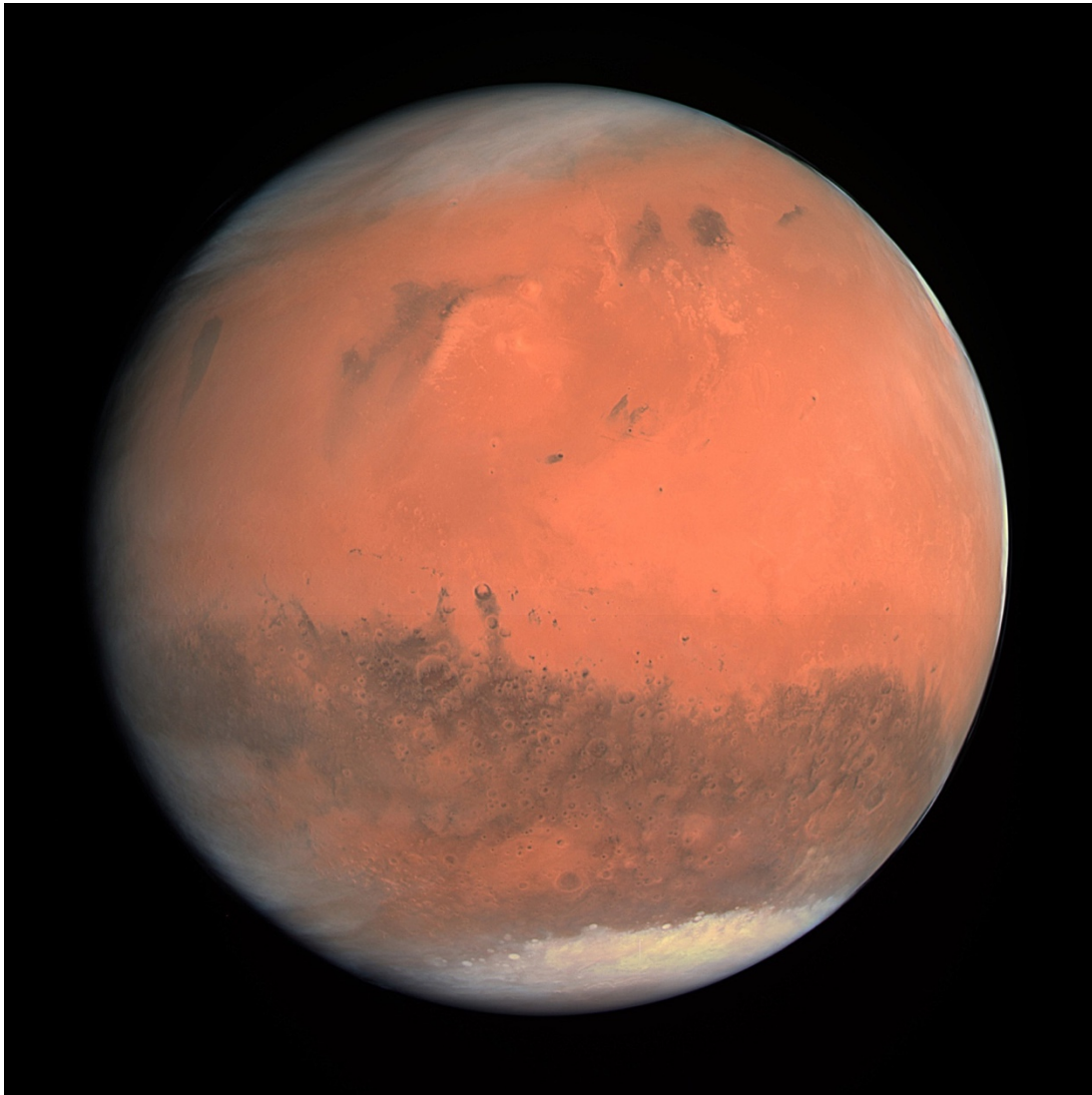


Figure 5. True color image of Mars taken by the OSIRIS instrument on the ESA Rosetta spacecraft during its February 2007 flyby of the planet. The image was generated using the OSIRIS orange (red), green, and blue filters. Courtesy of ESA & MPS for OSIRIS Team MPS/UPD/LAM/IAA/RSSD/INTA/UPM/DASP/IDA, CC BY-SA 3.0 IGO

Plate tectonics theory [26, 27], a modernized form of Wegener’s continental drift theory [28-30], represents attempts to describe Earth’s dynamics by observations of its surface. Plate tectonics, however, is a flawed theory: Plate tectonics theory is based upon the *planetesimal* theory of solar system formation, which does not account for the internal energy sources necessary to power plate mobility. By contrast, evidence validates the *protoplanetary* theory of

solar system formation which in fact provides two powerful internal energy sources, the stored energy of protoplanetary compression and georeactor nuclear fission energy [25]. Moreover, plate tectonics theory is predicated upon the critical assumption of mantle convection, which is physically-impossible for the following reason: Because of compression by the weight above, the bottom of the mantle is 62% denser than the surface. Decreasing mantle bottom density by thermal expansion (<1%) cannot make the mantle top-heavy as required for convection [7]. Additionally, other *ad hoc* assumptions are necessary to make plate tectonics seem to describe geological observations. For example, mountain ranges that predate the assumed collision-formation of Pangea, require the assumption of fictitious supercontinent cycles [31].

Whole-Earth Decompression Dynamics, the underlying basis of most geology, geophysics and surface phenomena, poses logically related explanations for geological observations usually attributed to plate tectonics without requiring mantle convection. Whole-Earth Decompression Dynamics is predicated upon the understanding that Earth had fully condensed as a Jupiter-like gas giant when the sun's thermonuclear reactions ignited and the resulting T-Tauri solar winds stripped the ices and gases from Earth's surface [1, 12, 15, 32, 33]. Earth's internal energy sources are a consequence of Earth's protoplanetary formation [25].

WHOLE-EARTH DECOMPRESSION DYNAMICS

Earth's Internal Energy Sources

Earth's condensation from within a giant gaseous protoplanet resulted in its inner 82% existing in a highly-reduced state of oxidation. Because of its oxygen-poor environment, uranium concentrated in the fluid core, instead of mantle silicates. The uranium precipitated and settled at the center of Earth where it functions as a self-regulating nuclear fission breeder reactor, called the georeactor [9-17], schematically illustrated in Figure 1. If Earth's magnetic field is generated by a convection-driven dynamo, magnetic amplifier, as suggested by Elsasser [32], it is produced by the georeactor [13, 17], not in the Earth's fluid core where convection is physically impossible [7]. Generally, planetocentric nuclear fission reactors are the basis for magnetic field generation in planets and large moons [33, 34].

The gases and ices of Earth's complete condensation as a Jupiter-like gas giant amounted to about 300 Earth-masses. This massive weight compressed the rocky portion to about two-thirds Earth's present diameter and emplaced within it the tremendous energy of protoplanetary compression. After being stripped of its gases and ices by the violent solar wind produced during thermonuclear ignition of the sun, over time Earth began to decompress. Whole-Earth Decompression Dynamics describes the geological and geophysical consequences of Earth's decompression [1, 12, 15, 35, 36].

The stored energy of protoplanetary compression is the primary energy source for decompression. However, for decompression to progress without cooling and impeding decompression, the lost heat of compression must be supplied by georeactor nuclear fission and radioactive decay energy. In addition to doing work against gravity, the stored energy of protoplanetary compression heats the base of the crust by a process known as *mantle decompression thermal tsunami* [37]. Decompression beginning within Earth's mantle propagates outward like a wave through silicates of decreasing density until it reaches the rigid crust where compression and compression heating takes place. That compression heating is

the heat source for the geothermal gradient as well as for other surface phenomena including shallow-source volcanoes. The geothermal gradient, produced by mantle decompression thermal tsunami, poses a barrier to the downward percolation of ground water.

In addition to replacing the lost heat of protoplanetary compression and powering the geomagnetic field, georeactor fission-produced heat is channeled to the surface along with its signature-helium isotopes forming deep-source volcanoes. Examples of these include the Hawaiian Islands and Iceland [38], Deccan traps [39] and Siberian traps [40].

Earth's Surface Manifestations

During Earth's decompression its surface area must increase and its surface curvature must adjust. As described by Whole-Earth Decompression Dynamics, during decompression Earth's surface area increases by the formation of decompression cracks, *primary* decompression cracks are underlain by heat sources that extrude basalt which eventually falls into and fills *secondary* decompression cracks that are devoid of underlying heat sources. This process, illustrated schematically in Figure 6 is responsible for the topography of the ocean floors. Indeed, all ocean-floor evidence arrayed to support plate tectonics supports Whole-Earth Decompression Dynamics, which does not require physically-impossible mantle convection.

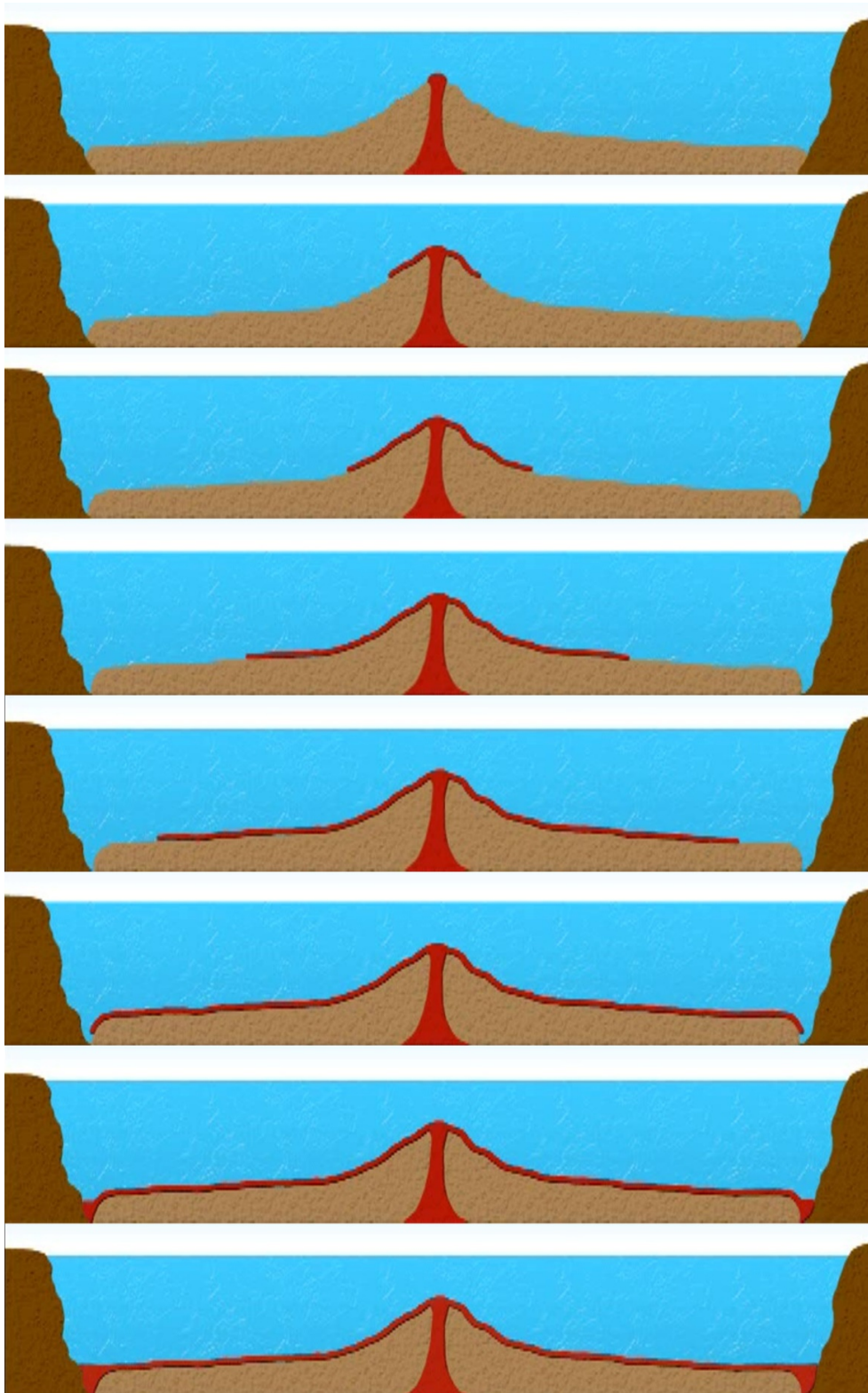


Figure 6. Top to bottom schematic image of the Whole-Earth Decompression Dynamics process of increasing Earth's surface area by the formation of ocean basins. Courtesy of Seyo Cizmic

Mid-oceanic ridges are examples of the primary decompression cracks. Circum-Pacific trenches are examples of secondary decompression cracks. Oceanic troughs, inexplicable in plate tectonics, are partially in-filled secondary decompression cracks.

The mechanism responsible for changes in Earth's surface curvature during whole-Earth decompression, illustrated in Figure 7, primarily results in the formation of mountain ranges characterized by folding [36, 41] and secondarily results in the formation of fjords and submarine canyons [42].

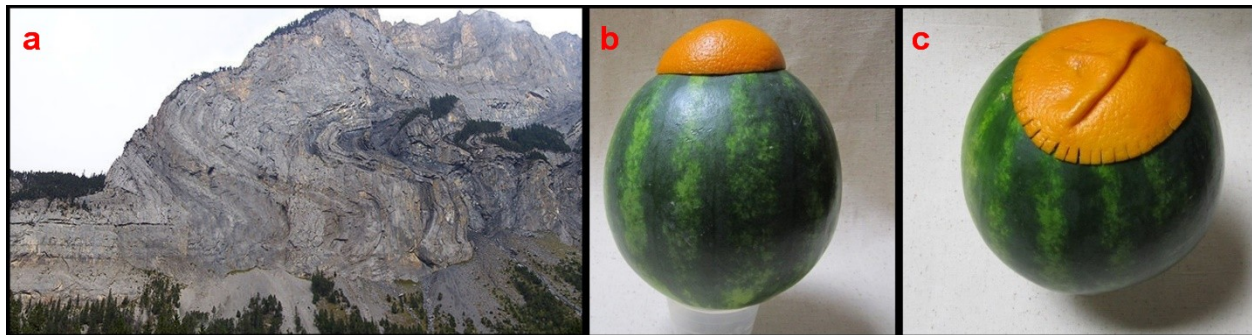


Figure 7. (a) Example of mountain folding; (b) The necessity for surface curvature change during whole-Earth decompression. The un-decompressed Earth is represented by the orange; the larger, decompressed Earth, is represented by the melon. Note the curvatures do not match; (c) Two causally-related curvature-change mechanisms that naturally result in surface curvature change, namely, major curvature adjustment by folded-over tucks, minor curvature adjustment by continental-perimeter tears. From [41]

WHOLE-MARS DECOMPRESSION DYNAMICS

Evidence that Mars had an internally generated magnetic field early in its lifetime [43-45] is evidence that interior portions of Mars experienced protoplanetary condensation. In the highly reducing solar matter environment at high pressures and high temperatures, molten iron and all of the elements dissolved in it including uranium, is the first major condensate to rain-out directly forming the core. Planetocentric nuclear fission reactors, self-regulating and producing planetary magnetic fields, are the inevitable consequence of protoplanetary condensation, including Mars.

Evidence of Whole-Mars Decompression Dynamics is not generally as conspicuous as the mountain ranges characterized by folding on Earth or the circum-Pacific trenches. However, one extremely prominent feature of Mars represents an outstanding example. Valles Marineris, in the southern hemisphere, is a set of partially in-filled secondary decompression cracks 150-2200 km long, 75-150 km wide, and at least 5-10 km deep [46-48]. As a consequence of whole-Mars decompression increased diameter, these decompression cracks necessarily formed to increase the surface area correspondingly.

According to the National Aeronautics and Space Administration (NASA), Figure 8 is a mosaic of the Valles Marineris hemisphere of Mars projected into point perspective, a view similar to that which one would see from a spacecraft. The distance is 2500 km from the surface of the planet, with a scale being 0.6km/pixel. The mosaic is composed of 102 Viking Orbiter images of

Mars. The center of the scene (latitude -8, longitude 78) shows the entire Valles Marineris secondary decompression crack system.

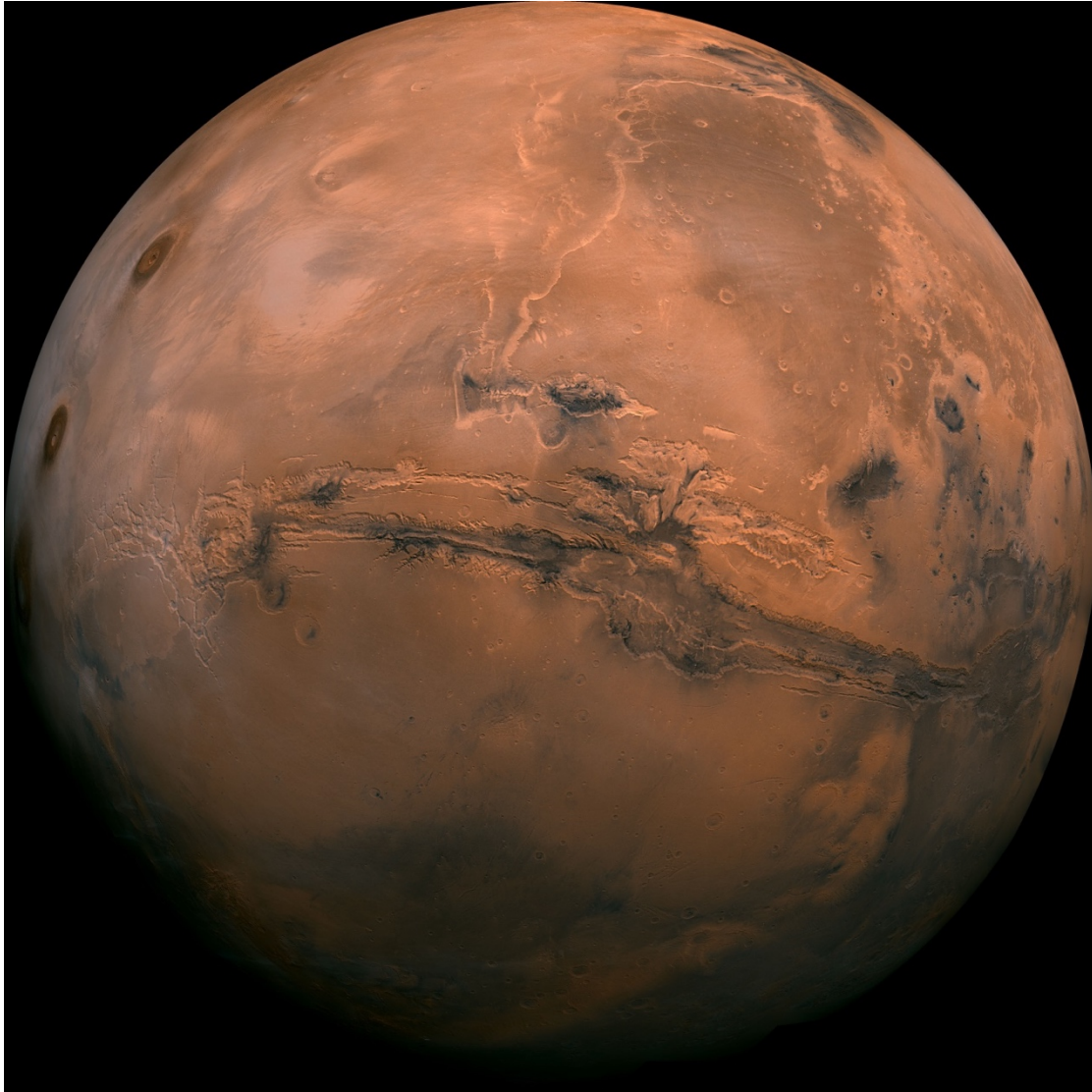


Figure 8. Mosaic of the Valles Marineris hemisphere of Mars. NASA image.

Figure 9 is a Mercator map of Mars onto which I added names of prominent, related features.

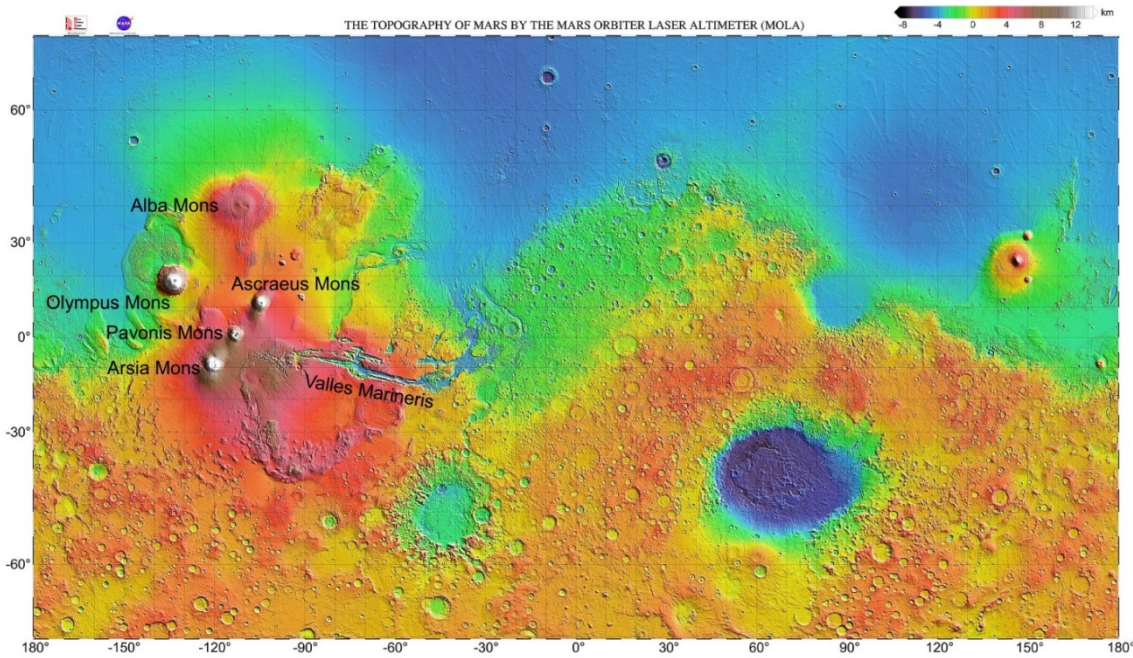


Figure 9. Mercator map showing the concentration of volcanoes near Valles Marineris

Figure 10 is a mosaic image of Valles Marineris – colored to resemble the Martian surface – derived from the Thermal Imaging System (THEMIS), a visible-light and infrared-sensing camera on NASA’s Mars Odyssey orbiter. Produced from more than 500 daytime infrared photos, the mosaic shows the whole valley in more detail than any previous composite photo. The smallest details visible in the image are about the size of a football field, 100 meters.

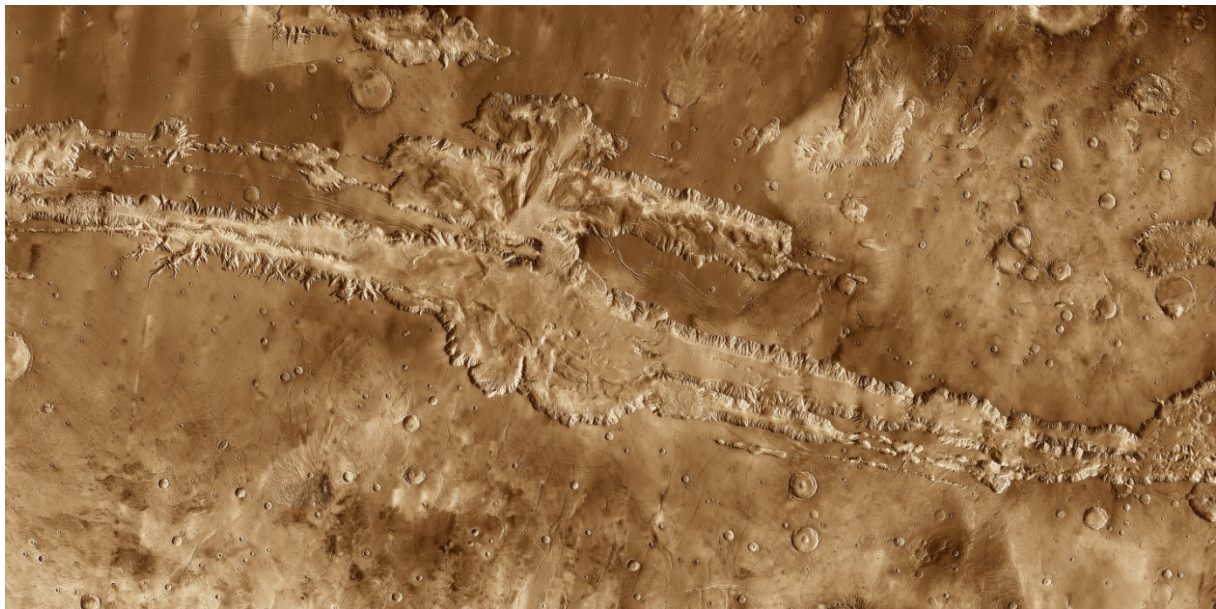


Figure 10. Mosaic image of Valles Marineris, artificially colored, constructed from more than 500 daytime infrared photos. NASA image

During whole-Mars decompression, (1) surface cracks form that are subsequently in-filled to increase surface area, and (2) surface curvature adjustments must be made. The upper image in Figure 11 is a magnified view of a section of Figure 10 showing in greater detail the perimeter-features common to the partially in-filled secondary decompression cracks of Valles Marineris. The inset in the upper image from Figure 7c serves as a reminder of two means of surface curvature adjustment. To date, no evidence of Martian mountains characterized by folding has been reported. However, the common perimeter-features of Valles Marineris, I posit, are perimeter-tears like those of the Norwegian fjords [42] as shown by the lower images of Figure 11. Those perimeter-tears are indications of Martian surface curvature adjustments.

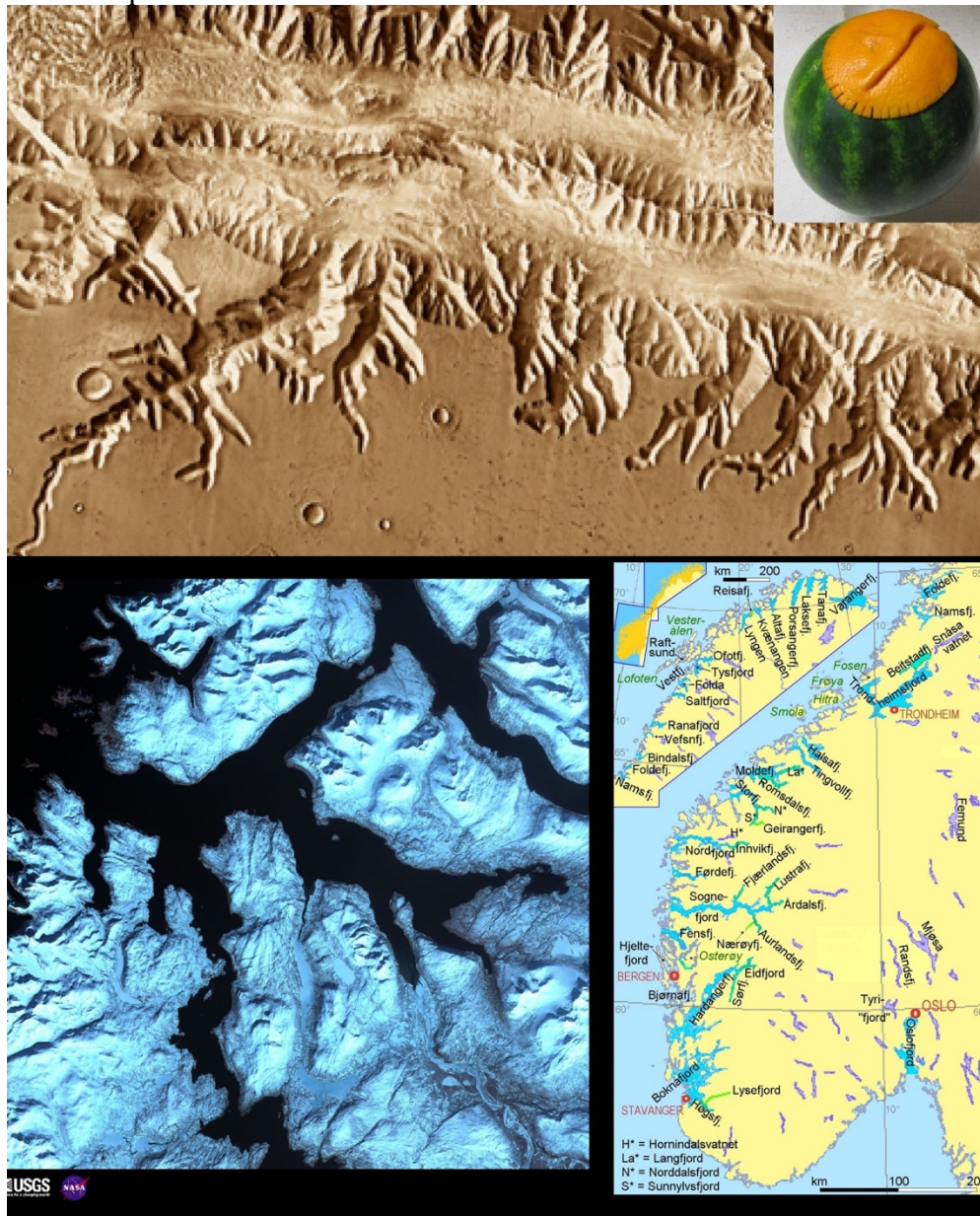


Figure 11. Upper: Magnified section of Figure 8, Valles Marineris, showing circum-perimeter tears, with inset from Figure 7c illustrating mechanisms for surface curvature adjustments; Lower: USGS/NASA satellite view of the northern portion of Norway showing fjords and map of Norway showing fjords, from [42]

Figure 12 shows two rimless pits located to the northwest of Ascreaus Mons. The pits are 180 and 310 meters in diameter. The associated wispy, dark material appears to have blown out of the pits. Although the Martian pits are considerably larger and far fewer than the pits on Mercury discovered by the Project Messenger mission [49], I suspect that they may be of similar origin, namely the result of hydrogen geysers [50]. Molten iron, which dissolves copious amounts of hydrogen, is the first major condensate during protoplanetary formation. Eventually, when the planetary core solidifies, the hydrogen is exsolved and rushes to the surface. Along the way the hydrogen reduces iron sulfide to iron metal, which is blown out and deposited at the surface. On Mercury, which is devoid of atmospheric winds, the iron is deposited around the pits and remains in its reduced state (Figure 13). On Mars, presumably the iron is blown downwind and becomes oxidized. In each case, the validity of this concept can be tested by determining whether the deposited material is iron metal and iron oxide, respectively.

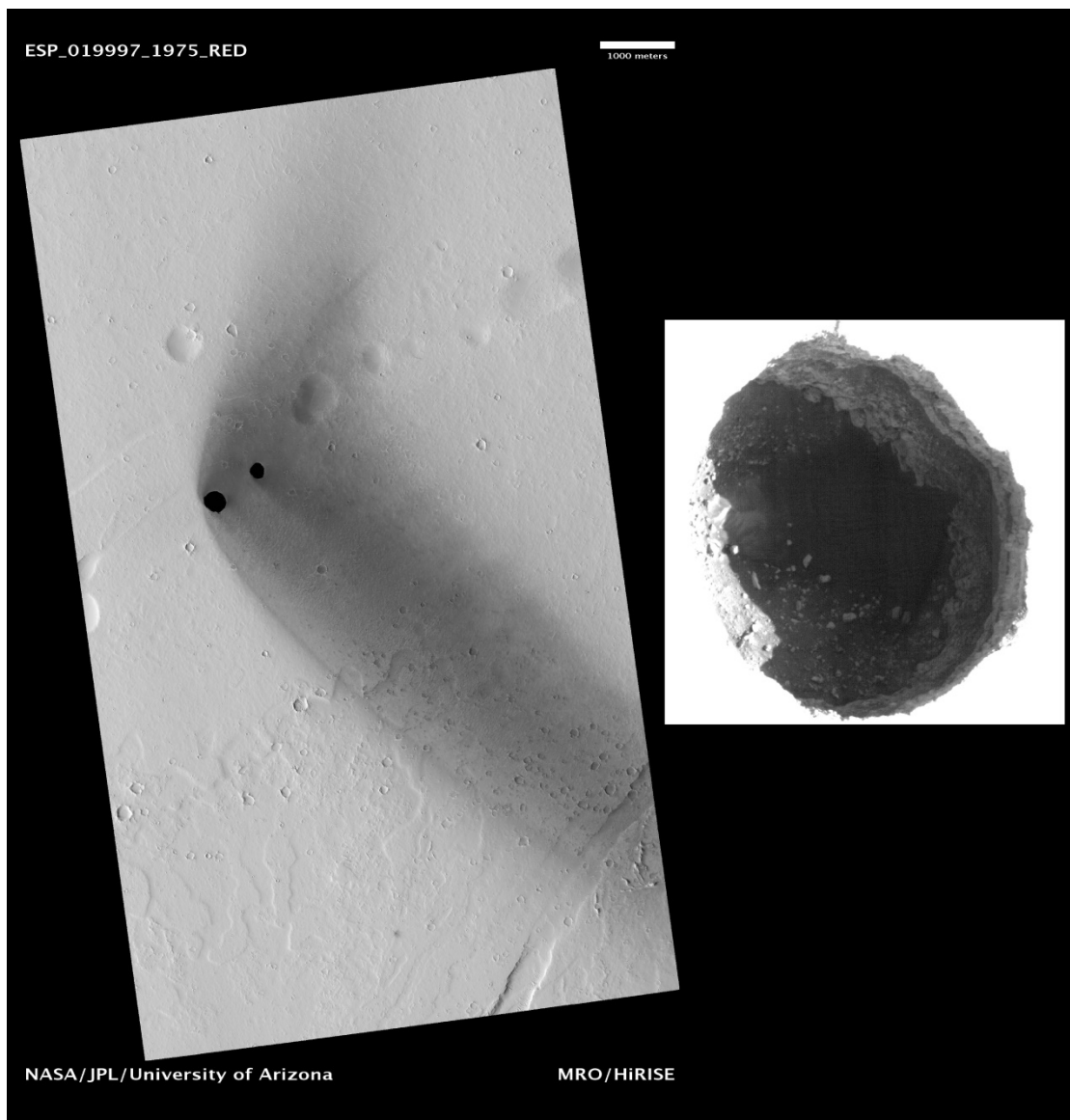


Figure 12. Dark rimless pits NW of Ascreaus Mons. Inset: Close up of rimless pit

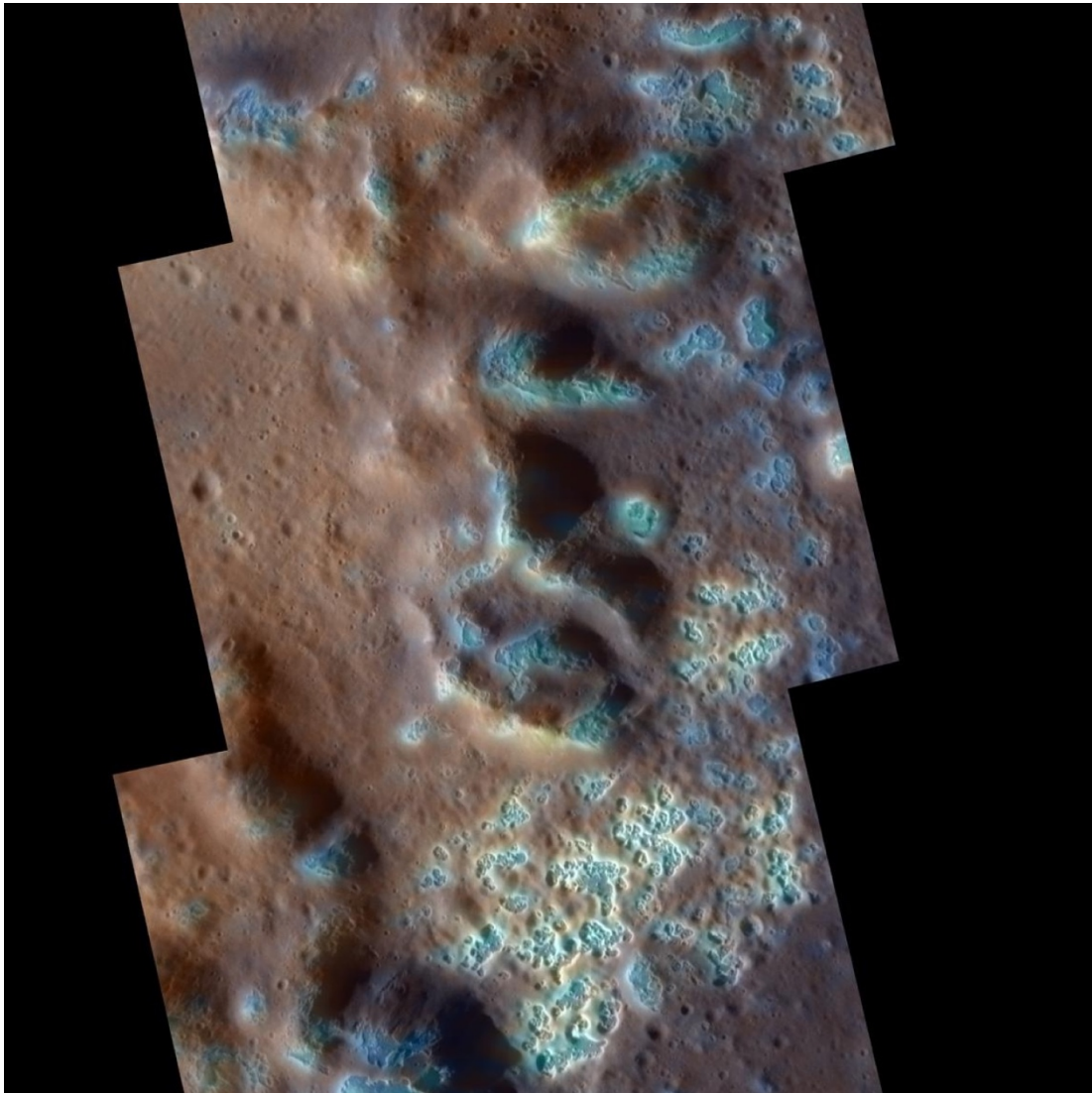


Figure 13. Pits surrounded by shiny material on planet Mercury. From [49]

WHERE TO LOOK FOR MARTIAN ORGANIC COMPOUNDS

If evidence of extra-terrestrial life is to be found in the solar system, Mars is the most likely place to look. Indeed, the primary focus of space agencies' exploration has been to seek likely regions, such as those revealing evidence of past flowing water [51]. An alternative approach is to seek the sources of Martian methane [52]. In an article published in the *Journal of Petroleum Exploration and Production Technology*, I described the scientific basis and evidence for a "New Concept on the Origin of Petroleum and Natural Gas" that follows from Whole-Earth Decompression Dynamics [53]. Based on these inferences, I suggest appropriate places to look for trapped organic compounds that might have arisen from whole-Mars decompression.

Whole-Earth decompression currently is operating, although less violently than in the past. A notable example is the East African Rift System shown with its associated volcanoes in Figure 14. The volcanoes associated with the East African Rift System are powered by heat channeled from the georeactor, as known by the isotopic signature helium that makes its way to the surface rocks through those heat channels. It is worthwhile to enquire whether the heat that

produced the volcanoes associated with Valles Marineris is likewise of nuclear reactor origin, as can be ascertained by making helium isotopic measurements on samples shielded from solar wind implanted helium. If so, then it might be prudent to seek organic deposits where life might have originated that are associated with the Valles Marineris region. Why? The East African Rift System (Figure 14) and the Siberian Traps (Figure 15) have extensive oil and natural gas deposits [53].



Figure 14. Northeastern portion of Africa. Red lines show the major decompression cracks comprising the East African Rift System. Active volcanoes are indicated by maroon triangles, oil discoveries by pluses [53, 54]

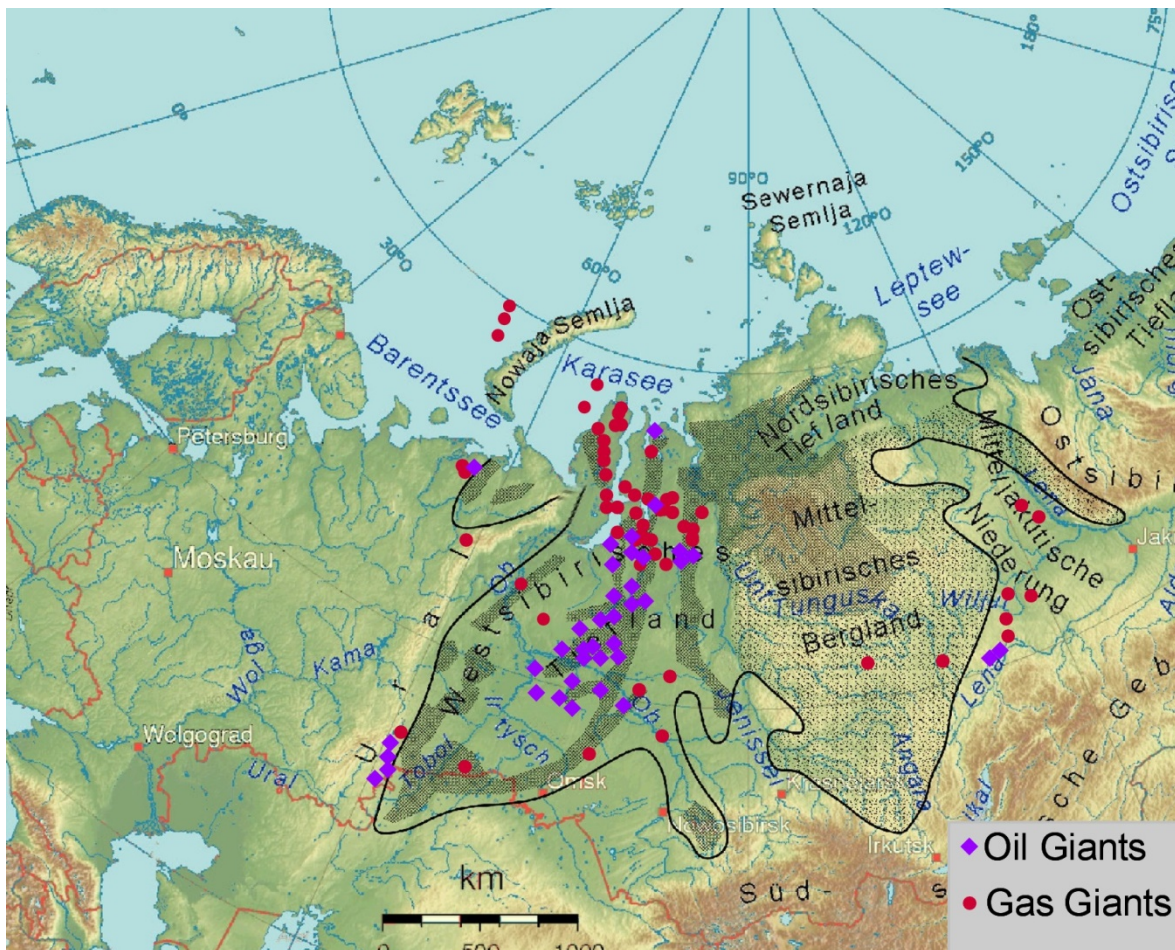


Figure 15. Map, courtesy of Jo Weber, showing the extent of the Siberian Traps as based upon estimates derived from Masaitis [55]. Circles show major gas fields; diamonds show major oil fields; data from Horn [56]. From [53]

MARS MANTLE DECOMPRESSION THERMAL TSUNAMI

Whole-Earth decompression progressed far more energetically than whole-Mars decompression. Based upon relative planetary masses, the Martian protoplanetary kernel was much smaller than that of Earth, <11%. The early demise of Mars' magnetic field [43-45] is consistent with a much smaller planetocentric nuclear fission reactor. The much less extensive Whole-Mars Decompression Dynamics is also a consequence of its being compressed by a less massive shell of ices and gases, <11% that of Earth.

Since 1939, scientists have been measuring the heat flowing out of Earth's continental crust [57, 58] and since 1952, the heat flowing out of ocean floor basalt far removed from mid-ocean ridges [59]. When the first heat flow measurements were reported on continental-rock, the heat was assumed to arise from radioactive decay. But then later, ocean floor heat flow measurements were made and what a surprise! There is more heat flowing out of the ocean floor than out of continental-rock. This was an enigma; ocean-floor basalt contains a much smaller percentage of radioactive elements than continental-rock. The solution to that enigma is the Whole-Earth Decompression Dynamics process called mantle decompression thermal tsunami.

Albeit controversial, there is evidence that during an early period on Mars there existed copious quantities of liquid water that was subsequently lost [60, 61]. However, so far, no one has published a holistic geological explanation for this postulation. How can the planet be initially warm and wet then change to cold and dry? The answer, I posit, is due to the Whole-Mars Decompression Dynamics process of mantle decompression thermal tsunami that while operating (1) heated the Martian surface and (2) provided a thermal barrier that prevented water from percolating too deeply underground. When mantle decompression thermal tsunami ceased, heat flow from the Martian surface subsided, and water encountered no thermal barrier to downward percolation. Presumably, this event was more or less contemporaneous with the demise of the planet's magnetic field which began the solar wind caused erosion of the Martian atmosphere [62].

CONCLUSIONS

Whole-Mars Decompression Dynamics, like Whole-Earth Decompression Dynamics, is based upon evidence that planets condensed from giant gaseous protoplanets which established their highly reduced internal compositions, their planetocentric nuclear fission reactors, and ultimately resulted in their formation as gas giants, surrounded by shells of ices and gases amounting to about 300 times the rocky planet mass. The resulting compression stored within the rocky planets a powerful energy source, the energy of protoplanetary compression. The super-intense T-Tauri phase solar winds accompanying thermonuclear ignition of the sun stripped away the gaseous envelopes thus beginning the process of whole-planet decompression.

Whole-Earth decompression progressed far more energetically than whole-Mars decompression. Based upon relative planetary masses, the Martian protoplanetary kernel was much smaller than that of Earth. The early demise of Mars' magnetic field is consistent with a much smaller planetocentric nuclear fission reactor. The much less extensive Whole-Mars Decompression Dynamics is also a consequence of Mars being compressed by a less massive shell of ices and gases. Nevertheless, surface evidence, notably Valles Marineris, is consistent with whole-Mars decompression.

Perhaps the most important consequence of Whole-Mars Decompression Dynamics is, through the process of mantle decompression thermal tsunami, the stored energy of protoplanetary compression also heated the crust and provided a thermal barrier to the downward percolation of water. Presumably contemporaneous with demise of the magnetic field, the whole-Mars decompression process subsided, concomitantly transforming Mars from warm and wet to cold and dry. Whole-Mars Decompression Dynamics provides different possible interpretations of Martian features and events, including the perimeter-features of Valles Marineris being circum-perimeter tears like Norwegian fjords, surface pits being the consequence of hydrogen geysers like on Mercury, and implications where one might hope to find Martian hydrocarbon deposits.

References

1. Herndon, J.M., *New indivisible planetary science paradigm*. Curr. Sci., 2013. 105(4): p. 450-460.
2. Eucken, A., *Physikalisch-chemische Betrachtungen ueber die fruehste Entwicklungsgeschichte der Erde*. Nachr. Akad. Wiss. Goettingen, Math.-Kl., 1944: p. 1-25.
3. Herndon, J.M. and H.E. Suess, *Can enstatite meteorites form from a nebula of solar composition?* Geochim. Cosmochim. Acta, 1976. 40: p. 395-399.
4. Herndon, J.M., *The chemical composition of the interior shells of the Earth*. Proc. R. Soc. Lond, 1980. A372: p. 149-154.
5. Herndon, J.M., *The object at the centre of the Earth*. Naturwissenschaften, 1982. 69: p. 34-37.
6. Herndon, J.M., *Composition of the deep interior of the earth: divergent geophysical development with fundamentally different geophysical implications*. Phys. Earth Plan. Inter, 1998. 105: p. 1-4.
7. Herndon, J.M., *Geodynamic Basis of Heat Transport in the Earth*. Curr. Sci., 2011. 101(11): p. 1440-1450.
8. Herndon, J.M., *Reasons why geomagnetic field generation is physically impossible in Earth's fluid core*. Advances in Social Sciences Research Journal, 2021. 8(5): p. 84-97.
9. Herndon, J.M., *Feasibility of a nuclear fission reactor at the center of the Earth as the energy source for the geomagnetic field*. J. Geomag. Geoelectr., 1993. 45: p. 423-437.
10. Herndon, J.M., *Planetary and protostellar nuclear fission: Implications for planetary change, stellar ignition and dark matter*. Proc. R. Soc. Lond, 1994. A455: p. 453-461.
11. Herndon, J.M., *Sub-structure of the inner core of the earth*. Proc. Nat. Acad. Sci. USA, 1996. 93: p. 646-648.
12. Herndon, J.M., *Nuclear georeactor origin of oceanic basalt $^3\text{He}/^4\text{He}$, evidence, and implications*. Proc. Nat. Acad. Sci. USA, 2003. 100(6): p. 3047-3050.
13. Herndon, J.M., *Terracentric nuclear fission georeactor: background, basis, feasibility, structure, evidence and geophysical implications*. Curr. Sci., 2014. 106(4): p. 528-541.
14. Hollenbach, D.F. and J.M. Herndon, *Deep-earth reactor: nuclear fission, helium, and the geomagnetic field*. Proc. Nat. Acad. Sci. USA, 2001. 98(20): p. 11085-11090.
15. Herndon, J.M., *Whole-Earth decompression dynamics*. Curr. Sci., 2005. 89(10): p. 1937-1941.
16. Herndon, J.M., *Mantle decompression thermal-tsunami*. arXiv: physics/0602085 13 Feb 2006, 2006.
17. Herndon, J.M., *Nuclear georeactor generation of the earth's geomagnetic field*. Curr. Sci., 2007. 93(11): p. 1485-1487.
18. Świeczak, M. and M. Grad, *Upper mantle seismic discontinuities topography variations beneath Eastern Europe*. Acta Geophys. Pol., 2004. 52(3): p. 252-270.
19. Dziewonski, A.M. and D.A. Anderson, *Preliminary reference Earth model*. Phys. Earth Planet. Inter., 1981. 25: p. 297-356.
20. Keil, K., *Mineralogical and chemical relationships among enstatite chondrites*. J. Geophys. Res., 1968. 73(22): p. 6945-6976.
21. Kennet, B.L.N., E.R. Engdahl, and R. Buland, *Constraints on seismic velocities in the earth from travel times*. Geophys. J. Int., 1995. 122: p. 108-124.
22. Birch, F., *Elasticity and constitution of the Earth's interior*. J. Geophys. Res., 1952. 57(227-286).
23. Herndon, J.M., *Discovery of fundamental mass ratio relationships of whole-rock chondritic major elements: Implications on ordinary chondrite formation and on planet Mercury's composition*. Curr. Sci., 2007. 93(3): p. 394-398.
24. Herndon, J.M., *Making sense of choondritic meteorites*. Advances in Social Sciences Research Journal, 2022. 9(2): p. 82-102.

25. Herndon, J.M., *Validation of the protoplanetary theory of solar system formation*. *Journal of Geography, Environment and Earth Sciences International*, 2022. 26(2): p. 17-24.
26. Oreskes, N. and H.E. LeGrand, *Plate tectonics: An insider's history of the modern theory of the Earth* 2001: Westview Press.
27. Cox, A. and R.B. Hart, *Plate tectonics: How it works* 2009: John Wiley & Sons.
28. Wegener, A., *Die Entstehung der Kontinente und Ozeane*. fourth ed 1929, Braunschweig: Friedr. Vieweg & Sohn. 246.
29. Wegener, A., *The Origin of Continents and Oceans*. Translated by John Biram 1966, New York: Dover Publications, Inc.
30. Wegener, A.L., *Die Entstehung der Kontinente*. *Geol. Rundschau*, 1912. 3: p. 276-292.
31. Herndon, J.M., *Fictitious Supercontinent Cycles*. *Journal of Geography, Environment and Earth Science International*, 2016. 7(1): p. 1-7.
32. Elsasser, W.M., *On the origin of the Earth's magnetic field*. *Phys. Rev.*, 1939. 55: p. 489-498.
33. Herndon, J.M., *Nature of planetary matter and magnetic field generation in the solar system*. *Curr. Sci.*, 2009. 96(8): p. 1033-1039.
34. Herndon, J.M., *Fictitious Supercontinent Cycles*. [arXiv.org/abs/1302.1425](https://arxiv.org/abs/1302.1425), 2013.
35. Herndon, J.M., *Whole-Earth decompression dynamics: new Earth formation geoscience paradigm fundamental basis of geology and geophysics*. *Advances in Social Sciences Research Journal*, 2021. 8(2): p. 340-365.
36. Herndon, J.M., *Origin of mountains and primary initiation of submarine canyons: the consequences of Earth's early formation as a Jupiter-like gas giant*. *Curr. Sci.*, 2012. 102(10): p. 1370-1372.
37. Herndon, J.M., *Energy for geodynamics: Mantle decompression thermal tsunamis*. *Curr. Sci.*, 2006. 90(12): p. 1605-1606.
38. Hilton, D.R., et al., *Extreme He-3/He-4 ratios in northwest Iceland: constraining the common component in mantle plumes*. *Earth Planet. Sci. Lett.*, 1999. 173(1-2): p. 53-60.
39. Basu, A.R., et al., *Early and late alkali igneous pulses and a high-³He plume origin for the Deccan flood basalts*. *Sci.*, 1993. 261: p. 902-906.
40. Basu, A.R., et al., *High-³He plume origin and temporal-spacial evolution of the Siberian flood basalts*. *Sci.*, 1995. 269: p. 882-825.
41. Herndon, J.M., *Formation of mountain ranges: Described By Whole-Earth Decompression Dynamics*. *Journal of Geography, Environment and Earth Science International*, 2022. 26(3): p. 52-59.
42. Herndon, J.M., *New Concept for the Origin of Fjords and Submarine Canyons: Consequence of Whole-Earth Decompression Dynamics*. *Journal of Geography, Environment and Earth Science International*, 2016. 7(4): p. 1-10.
43. Connerney, J., et al., *The global magnetic field of Mars and implications for crustal evolution*. *Geophysical Research Letters*, 2001. 28(21): p. 4015-4018.
44. Lillis, R.J., et al., *An improved crustal magnetic field map of Mars from electron reflectometry: Highland volcano magmatic history and the end of the Martian dynamo*. *Icarus*, 2008. 194(2): p. 575-596.
45. Lillis, R.J., et al., *Time history of the Martian dynamo from crater magnetic field analysis*. *Journal of Geophysical Research: Planets*, 2013. 118(7): p. 1488-1511.
46. Schultz, R.A., *Structural development of coprates chasma and western ophir planum, valles marineris rift, mars*. *Journal of Geophysical Research: Planets*, 1991. 96(E5): p. 22777-22792.
47. Andrews-Hanna, J.C., *The formation of Valles Marineris: 2. Stress focusing along the buried dichotomy boundary*. *Journal of Geophysical Research: Planets*, 2012. 117(E4).

-
48. Davis, J.M., et al., *A record of syn-tectonic sedimentation revealed by perched alluvial fan deposits in Valles Marineris, Mars*. *Geology*, 2021. 49(10): p. 1250-1254.
49. Blewett, D.T., et al., *Hollows on Mercury: MESSENGER Evidence for Geologically Recent Volatile-Related Activity*. *Science*, 2011. 333: p. 1859-1859.
50. Herndon, J.M., *Hydrogen geysers: Explanation for observed evidence of geologically recent volatile-related activity on Mercury's surface*. *Curr. Sci.*, 2012. 103(4): p. 361-361.
51. Orosei, R., et al., *The global search for liquid water on Mars from orbit: Current and future perspectives*. *Life*, 2020. 10(8): p. 120.
52. Oehler, D.Z. and G. Etiope, *Methane seepage on Mars: where to look and why*. *Astrobiology*, 2017. 17(12): p. 1233-1264.
53. Herndon, J.M., *New concept on the origin of petroleum and natural gas deposits*. *J Petrol Explor Prod Technol* 2017. 7(2): p. 345-352.
54. Herndon, J.M., *Herndon's Earth and the Dark Side of Science* 2014: Printed by CreateSpace; Available at Amazon.com and through other book sellers.
55. Masaitis, V.L., *Permian and Triassic volcanism of Siberia*. *Zapiski VMO*, 1983. part CXII(4): p. 412-425.
56. Horn, M.K., *Giant Fields 1869-2003*, in *Giant Oil and Gas Fields of the Decade, 1990-1999*, M.K. Halbouty, Editor 2003, AAPG: Houston.
57. Benfield, A.F., *Terrestrial heat flow in Great Britain*. *Proc. R. Soc. Lond*, 1939. Ser A 173: p. 428-450.
58. Bullard, E.C., *Heat flow in South Africa*. *Proc. R. Soc. Lond*, 1939. Ser. A 173: p. 474-502.
59. Revelle, R. and A.E. Maxwell, *Heat flow through the floor of the eastern North Pacific Ocean*. *Nature*, 1952. 170: p. 199-200.
60. Di Achille, G. and B.M. Hynek, *Ancient ocean on Mars supported by global distribution of deltas and valleys*. *Nature Geoscience*, 2010. 3(7): p. 459-463.
61. Nazari-Sharabian, M., et al., *Water on Mars—A Literature Review*. *Galaxies*, 2020. 8(2): p. 40.
62. Kass, D. and Y.L. Yung, *Loss of atmosphere from Mars due to solar wind-induced sputtering*. *Science*, 1995. 268(5211): p. 697-699.